Incorporation of a tilting coordinate into the multidimensional Langevin dynamics of heavy-ion-induced fission: Analysis of experimental data from fusion-fission reactions

P. N. Nadtochy, E. G. Ryabov, A. E. Gegechkori, Yu. A. Anischenko, and G. D. Adeev
Omsk State University, Mira prospekt 55-A, Omsk, 644077, Russia
(Received 19 November 2013; published 29 January 2014)

A four-dimensional dynamical model was developed and applied to study fission characteristics in a wide range of a fissility parameter. Three collective shape coordinates and the K coordinate were considered dynamically from the ground-state deformation to the scission into fission fragments. A modified one-body mechanism for nuclear dissipation with a reduction coefficient k_s of the contribution from a "wall" formula has been used in the study. The inclusion of the K coordinate in the dynamical consideration and use of the "chaos-weighted wall formula" with a deformation-dependent scaling factor $k_s(q_1)$ lead to fairly good reproduction of the variances of the fission-fragment mass distribution and the prescission neutron multiplicity for a number of fissioning compound nuclei in a wide fissility range. The four-dimensional dynamical calculations describe better experimental prescission neutron multiplicity and variances of fission-fragment mass distribution for heaviest nuclei with respect to a three-dimensional dynamical model, where the K coordinate is assumed to be equal to zero. The estimate of a dissipation coefficient for the orientation degree of freedom, $\gamma_K \simeq 0.077$ (MeV zs)$^{-1/2}$, is good for heavy nuclei and a larger value of $\gamma_K \simeq 0.2$ (MeV zs)$^{-1/2}$ is needed for nuclei with mass $A_{\rm CN} \simeq 200$.

DOI: 10.1103/PhysRevC.89.014616 PACS number(s): 25.85.−w, 05.10.Gg, 25.70.Jj

I. INTRODUCTION

During the past decades different methods of dynamical consideration of the fission process have been extensively and rather successfully applied to elucidate many problems of collective nuclear dynamics [1–5]. In the high-excitation-energy region numerous multidimensional Langevin calculations based on a phenomenological description of transport coefficients [2,6–12] have proven capable of reproducing fission experimental data in a wide range of the compound nucleus fissility parameter. Recently, the significance of the orientation degree of freedom (the tilting mode or K coordinate), which is the projection of the total angular momentum (I) onto the symmetry axis of the fissioning nucleus, was demonstrated with respect to both statistical and dynamical considerations of the fission process [13–15]. At present, many models do not consider the evolution of the K coordinate, and it is assumed to be fixed to zero. However, in order to calculate the angular distribution of fission fragments the equilibrium distribution of the K coordinate at the transition state (at the saddle or scission point) is assumed. Therefore, recently, a three-dimensional (3D) dynamical model was elaborated to take into account the fourth collective coordinate (K coordinate) [15] that could substantially influence the dynamical evolution of the fissioning system and predict the parameters of the mass-energy distribution (MED) of fission fragments as well as the fission time scale [14,15]. Inclusion of this coordinate into the 3D dynamical model allowed the first unification of the dynamical description of the MED and the angular distribution of fission fragments.

Eremenko and co-authors [16,17] were the first to consider the evolution of the orientation degree of freedom of the fissioning nucleus as an independent collective coordinate, using a Monte Carlo method implemented for simulation of the Anderson-Kubo process. They were able to describe successfully the angular distributions of fission fragments and mean multiplicities of prescission neutrons for a number of fusion-fission reactions involving heavy ions. Karpov and co-authors [18,19] combined their idea with the 3D Langevin dynamical calculations [20,21], employing a Metropolis algorithm instead of the Andersen-Kubo process. The dynamical aspects of the angular distribution formation have been evaluated using the tilting mode relaxation time τ_K. In Refs. [16,17] the dynamical treatment of the tilting mode was joined with one-dimensional Langevin dynamics for the shape degree of freedom, whereas the 3D Langevin equations were employed, as was mentioned above, in Refs. [18,19]. The K equilibration time τ_K is deduced to be 20–30 zs in Refs. [16,17] and 2–4 zs in Refs. [18,19] from the fits of calculated values to experimental data on anisotropy of the angular distribution for heavy fissioning compound systems with mass $A_{\rm CN} \simeq 220$–250.

An alternative method for considering the evolution of the K coordinate was proposed by Lestone [13] and further developed by Lestone and McCalla [14]. They described the evolution of the K coordinate with the overdamped Langevin equation. The Langevin equation for the K coordinate makes it possible to simulate the relaxation of K states with allowance for the instantaneous physical properties of the fissioning system, such as its temperature and moment of inertia, instead of treating the respective relaxation time as a free parameter [16–19]; moreover, it describes the evolution of all collective degrees of freedom of the nucleus within a unified conceptual framework. Thus, the Langevin dynamics of fission induced by heavy ions must include at least four collective coordinates—three for the evolution of the nuclear shape [2,20,21] and one for the evolution of the tilting mode [13–19,22,23].

The first results of the dynamical calculations based on the 3D Langevin model plus the K coordinate (4D) [15] demonstrated the advantage of such an approach, because the 4D dynamical model allows consistent calculations of

fission-fragment MED, the angular distribution of fission fragments, and prescission particle multiplicities. The calculations performed in Ref. [15] have shown that the 4D model could describe the fission-fragment MED parameters and prescission particles multiplicities for heavy nuclei using almost the same dissipation strength, which is not possible within the 3D calculations. It should be noted that the 4D calculations in [15] have been performed only for two rather heavy compound fissioning nuclei, namely, ^{224}Th and ^{248}Cf. Certainly, the 4D calculations similar to those in Ref. [15] should be extended to compound nuclei with lower value of the fissility parameter. In the present study we investigate in detail the influence of the K coordinate on the fission rate, time scale, and fission observables in a wide range of fissility parameter. The results of the present study could be valuable for the qualitative estimations of the K-coordinate effects in the models that do not consider this coordinate.

The paper is organized as follows. Section II describes the 4D Langevin model, including its basic equations, input parameters, and details of calculations. Section III presents the results obtained from the application of the developed model. Finally, Sec. IV contains closing remarks.

II. MODEL

In the present study we applied a stochastic approach to treat the fission process at high excitation energy [1,24–26]. For the dynamical description of the fissioning nucleus shape evolution we used the recently developed 4D Langevin dynamical model. The detailed description of the model can be found in Ref. [15], and here we only give a short description of its basic ingredients.

We employed a $\{c,h,\alpha\}$ parametrization [27] for the generation of a nuclear shape. In this parametrization c is the elongation parameter; h describes the variation in the thickness of the neck for a given elongation of the nucleus; and the mass asymmetry parameter α determines the ratio of the nascent fission-fragment volumes.

In the stochastic approach, the evolution of the collective coordinates is considered as the motion of Brownian particles, which interact stochastically with a large number of internal degrees of freedom constituting the surrounding "heat bath." The coupled Langevin equations for the description of the dynamics of the collective coordinates have the form

$$\begin{aligned}\frac{dq_i}{dt} &= \mu_{ij}p_j,\\ \frac{dp_i}{dt} &= -\frac{1}{2}p_j p_k\frac{\partial\mu_{jk}}{\partial q_i} - \left(\frac{\partial F}{\partial q_i}\right)_T - \gamma_{ij}\mu_{jk}p_k + \theta_{ij}\xi_j(t),\end{aligned} \tag{1}$$

where $\mathbf{q}$ is the vector of collective coordinates, $\mathbf{p}$ is the vector of conjugate momenta, $F(\mathbf{q},K) = V(\mathbf{q},K) - a(\mathbf{q})T^2$ is the Helmholtz free energy, $V(\mathbf{q})$ is the potential energy, $m_{ij}(\mathbf{q})$ ($\|\mu_{ij}\| = \|m_{ij}\|^{-1}$) is the tensor of inertia, and $\gamma_{ij}(\mathbf{q})$ is the friction tensor. $\xi_j(t)$ is a random variable satisfying the relations $\langle\xi_i\rangle = 0$ and $\langle\xi_i(t_1)\xi_j(t_2)\rangle = 2\delta_{ij}\delta(t_1 - t_2)$. Thus, the Markovian approximation is assumed to be valid. The strength of the random force θ_{ij} is given by the Einstein relation $\sum\theta_{ik}\theta_{kj} = T\gamma_{ij}$. The temperature of the heat bath T was determined by the Fermi-gas model formula $T = (E_{\rm int}/a)^{1/2}$, where $E_{\rm int}$ is the internal excitation energy of the nucleus and $a(\mathbf{q})$ is the level-density parameter with the coefficients taken from the work of Ignatyuk and co-authors [28]. The repeated indices in the equations above imply summation over the collective coordinates. The three collective coordinates $\mathbf{q} = (q_1,q_2,q_3)$ are related to the shape parameters c, h, and α by $q_1 = f_1(c)$, $q_2 = f_2(c,h,\alpha)$, and $q_3 = f_3(c,h,\alpha)$. The explicit expressions for $f_1(c)$, $f_2(c,h,\alpha)$, and $f_3(c,h,\alpha)$ can be found in Refs. [2,15]. The advantage of using the collective coordinates $\mathbf{q}$ instead of the shape parameters (c,h,α) is discussed in Refs. [2,29].

The potential energy of the nucleus was calculated within the framework of a macroscopic model with a finite range of nuclear forces [30] using the parameters from Ref. [31]. The potential energy was obtained as a sum of the Coulomb energy, the generalized surface energy (the nuclear interaction energy), and the rotational energy. The inertia tensor was calculated by applying the Werner-Wheeler approximation for incompressible irrotational flow [32]. A modified one-body mechanism of nuclear dissipation [33–37] was employed to determine the dissipative part of the driving forces with a reduction coefficient from the "wall" formula k_s. The value $k_s = 1.0$ corresponds to the standard "wall" and "wall-plus-window" formulas [33,34,38], whereas the values $0.2 < k_s < 0.5$ allow one to reproduce different features of the MED and particle multiplicities in multidimensional Langevin calculations [2,21,39–43] and agree with other theoretical predictions [35,44–47].

The use of the reduction coefficient k_s as a variable parameter ruins the main advantage of the wall-and-window formalism, namely, the absence of any free parameters. However, in Refs. [45,48–50] it is argued that chaos-theory-related ideas [50] can be used to calculate the value of the reduction coefficient k_s from the wall formula as a function of deformation of the fissioning nucleus. The applications of this approach to calculate the coefficient $k_s(\mathbf{q})$ for studying different fission characteristics have been rather successful and have shown that such calculations yield almost the same results as those using the constant k_s coefficient from the interval $0.25 < k_s < 0.5$ [7,10,11].

In Fig. 1, we show the potential energy in the coordinates q_1 and q_2 for the case of $q_3 = 0$. The dashed line in this figure represents the mean trajectory [2,20] calculated under the assumption of a one-body mechanism of nuclear viscosity with $k_s = 0.25$, and the crosses mark the saddle point and nuclear ground state. In addition, this figure shows examples of nuclear shapes in the $\{c,h,\alpha\}$ parametrization. The calculations are performed using the ^{224}Th nucleus as an example.

Applying the 4D model to study MED of fission fragments and prescission particles multiplicities, we decided to use the elongation-dependent reduction factor of the contribution from the wall formula $k_s = k_s(q_1)$ in addition to the constant k_s values. To calculate this dependence we follow [45–51], relying on the idea that the reduction factor is related to the chaosity measure of the nucleon motion inside the nuclear shape during the compound nucleus shape evolution from the ground state to the scission. The explicit form of

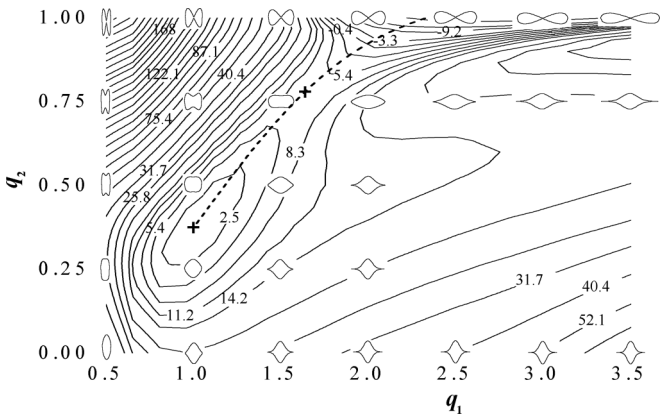

FIG. 1. The potential energy surface in the collective coordinates q_1 and q_2 at zero spin for the ^{224}Th nucleus ($q_3 = 0$) and the corresponding set of nuclear shapes. The crosses denote the ground state and the saddle point. The dashed line is the mean trajectory calculated under the assumption of the one-body mechanism of viscosity with $k_s = 0.25$. The numbers at the isolines correspond to the potential energy in MeV.

$k_s(q_1)$ was taken from [51]. Figure 2 shows the reduced friction coefficient $\beta_{q_2q_2} = \gamma_{q_2q_2}/m_{q_2q_2}$ for several values of the reduction coefficients k_s used in this study.

The description of the evolution of the K collective coordinate using the overdamped Langevin equation has been recently proposed in Ref. [14] as

$$\delta K = -\frac{\gamma_K^2 I^2}{2}\frac{\partial V}{\partial K}\delta t + \gamma_K I \xi \sqrt{T\delta t}, \tag{2}$$

where ξ is a random number from a normal distribution with unit variance. γ_K is a friction parameter controlling the coupling between the orientation degree of freedom K and the heat bath.

The Langevin equations for the shape parameters (1) and the Langevin equation for the K coordinate (2) are connected through the potential energy. The Langevin dynamics of the

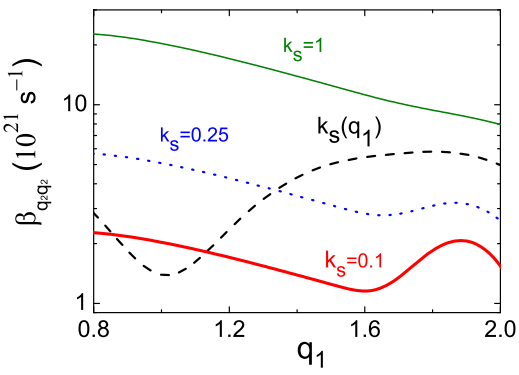

FIG. 2. (Color online) The reduced friction coefficient $\beta_{q_2q_2}$ as a function of elongation collective coordinate for the one-body dissipation mechanism with values of the reduction coefficient from the wall formula $k_s = 1$ (thin solid curve), 0.25 (dotted curve), and 0.1 (thick solid curve) and found on the basis of the "chaos-weighted wall formula" $k_s(q_1)$ (dashed curve) [51].

K coordinate is influenced by the actual value of the potential energy $V(\mathbf{q}, I, K)$. At the same time, the rotational part of the potential energy depends on the actual K value at time t, and in this way it influences the dynamical evolution of the shape parameters.

The rotational part of the potential energy is determined by the expression

$$E_{\rm rot}(\mathbf{q}, I, K) = \frac{\hbar^2 K^2}{2J_\parallel(\mathbf{q})} + \frac{\hbar^2[I(I+1) - K^2]}{2J_\perp(\mathbf{q})} = \frac{\hbar^2 I(I+1)}{2J_\perp(\mathbf{q})} + \frac{\hbar^2 K^2}{2J_{\rm eff}(\mathbf{q})}. \tag{3}$$

The functionals $J_\parallel$ and $J_\perp$ are the rigid-body moments of inertia, about and perpendicular to, the symmetry axis. Accounting for the diffuseness of the nuclear surface, one can calculate the moments of inertia as [52]

$$J_{\perp(\parallel)}(\mathbf{q}) = J_{\perp(\parallel)}^{\rm (sharp)}(\mathbf{q}) + 4M_0 a_M^2, \tag{4}$$

where $a_M = 0.704$ fm is the diffuseness parameter of the nuclear surface, M_0 is the compound nucleus mass, and $J_\perp^{\rm (sharp)}$ and $J_\parallel^{\rm (sharp)}$ are the moments of inertia for a sharp-edged nuclear density distribution. The effective moment of inertia is $J_{\rm eff}^{-1} = J_\parallel^{-1} - J_\perp^{-1}$. The expressions for $J_{\perp(\parallel)}^{\rm (sharp)}$ in the $\{c,h,\alpha\}$ parametrization can be found in [53].

Based on the works of Døssing and Randrup [54,55], Lestone and McCalla [14,56] have shown that, in the case of a dinucleus, γ_K can be expressed as

$$\gamma_K = \frac{1}{R_N R_{\rm cm}\sqrt{2\pi^3 n_0}}\sqrt{\frac{J_\parallel |J_{\rm eff}| J_R}{J_\perp^3}}, \tag{5}$$

where R_N is the neck radius, $R_{\rm cm}$ is the distance between the centers of mass of the nascent fragments, n_0 is the bulk flux in standard nuclear matter (0.0263 MeV zs fm^{-4}) [55], and $J_R = M_0 R_{\rm cm}^2/4$ for a reflection-symmetric shape. In a limiting case $\gamma_K \to 0$ and with an initial K value equal to zero, the present 4D Langevin model is reduced to the 3D model [2,20,21].

The deformation dependence of the dissipation coefficient γ_K given by Eq. (5) should be used with caution, as stated in Ref. [14], because Eq. (5) was obtained by assuming the nuclear shapes featuring a well-defined neck. Therefore, following Ref. [14], we choose γ_K to be a constant equal to 0.077 (MeV zs)$^{-1/2}$. Our previous calculations show that $\gamma_K \simeq 0.077$ (MeV zs)$^{-1/2}$ is appropriate for the description of the anisotropy of the angular distribution for the highly excited fissioning compound nuclei with mass $A_{\rm CN} \simeq 225$–250. This estimation has been obtained by using Eq. (5) for elongated nuclear shapes featuring a neck, which corresponds to the deformations typical for the descent from saddle to scission point. The above-mentioned value of the friction parameter γ_K used in [13,14] was obtained by Lestone and co-authors in their early study [57] from an analysis of the fission-fragment angular distribution measured for a number of fusion-fission reactions. This value was further used in Refs. [13,14] in the calculations of the mean fission time of excited compound nuclei.

The evaporation of the prescission light particles (n,p,α,γ) along the Langevin fission trajectories was taken into account by using a Monte Carlo simulation technique [58]. The spin I for each Langevin trajectory has been sampled from the spin distribution function

$$\sigma(I) = \frac{2\pi}{k^2}\frac{2I+1}{1+\exp[(I-I_c)/\delta I]}, \tag{6}$$

where k, I_c, and δI are the wave number, critical spin for fusion, and diffuseness, respectively. In the first approximation, I_c and δI values were defined according to the scaled prescription [26], which reproduces to a certain extent the dynamical results of the surface friction model [59] for the fusion of two heavy ions. Finally, the quantities I_c and δI were constrained from the experimental fusion cross section and $\langle I^2\rangle$. In the present study, we neglected the spins of the projectile and target nuclei and assumed that the spin of the compound nucleus, I, is approximately equal to the orbital angular momentum L. The initial K value was generated by using the Monte Carlo method from a uniform distribution in the interval $[-I,I]$ [14,17]. The initial conditions for the shape coordinates were chosen as follows. We started modeling fission dynamics from the ground state of the compound nucleus, with thermalized internal degrees of freedom. It was supposed that the scission occurred when the neck radius of the fissioning nucleus was equal to $0.3R_0$ [27,60] (where R_0 is the radius of the initial spherical nucleus). This scission condition determines the scission surface in the multidimensional space of collective coordinates. The Langevin trajectory determines the shape of the fissioning nucleus at the moment of scission into fragments by crossing the scission surface. The dynamical trajectory will either reach the scission surface, in which case it is counted as a fission event, or if the excitation energy for a trajectory which is still inside the saddle reaches the value $E_{\rm int} + E_{\rm coll}(\mathbf{q},\mathbf{p}) < \min(B_j,B_f)$ (where B_j is the binding energy of the particle $j = n,p,\alpha,\gamma$), the event is counted as an evaporation residue. The angular momentum lost by the compound nucleus in the evaporation process was determined under the assumption that the angular momentum carried away by the evaporated light particles is $I_j = 1$, 1, 2, and $1(\hbar)$ [26]. After the evaporation of the prescission particle we recalculated the excitation energy, spin, and all the dimensional factors entering the expressions for potential energy, mass, and friction tensors. The dynamical equations (1) and (2) were integrated simultaneously with the same time step until the scission or evaporation residue condition occurred. Correspondingly, the ensemble of sampled Langevin trajectories determines the ensemble of fission fragments and evaporation residues nuclei, and one can obtain the observables of interest, typical for full fission (FF) or evaporation residue (ER) channels, such as masses and kinetic energies of fission fragments, K values, temperatures, etc.

In the standard theoretical approach, fission fragments are assumed to be emitted along the direction of the nuclear symmetry axis at the transition-state configuration. The angular distribution in this case is given by [61,62]

$$W(\theta,I,K) = (I+1/2)\left|D^I_{M,K}(\theta)\right|^2, \tag{7}$$

where quantum number M is the projection of the total spin I on the space-fixed axis; θ is the angle with respect to the space-fixed axis; and $D^I_{M,K}(\theta)$ is the symmetric-top wave function. In case of zero spin target and projectile nuclei, M is zero, and the angular distribution of fission fragments is determined by averaging the expression (7) over the ensemble of Langevin trajectories

$$W(\theta) = \frac{1}{N_f}\sum_{j=1}^{N_f}(I^j+1/2)\left|D^{I^j}_{0,K^j}(\theta)\right|^2, \tag{8}$$

where the upper index j determines the value of the corresponding quantity at the scission point for the jth Langevin trajectory and N_f is the total number of simulated trajectories. Applying Eq. (8) within the present 4D calculations we determine the angular distribution at the scission surface. At the same scission point we also determine the masses and kinetic energy of fission fragments [43]. This procedure does not need the standard transition-state model assumptions on equilibration of a tilting mode at any arbitrary transition point, because the K coordinate is determined dynamically at every time step.

Additionally, the standard transition-state model has been used to analyze fission-fragment angular distributions. These calculations have been performed to compare the predictions of widely used transition-state models with the present dynamical model.

The angular distribution of fission fragments can be obtained by averaging Eq. (7) over the quantum numbers I and K:

$$W(\theta) = \sum_{I=0}^{\infty}\sigma(I)\sum_{K=-I}^{I}P_I(K)W(\theta,I,K). \tag{9}$$

It is seen from Eq. (9) that for the calculation of the angular distribution it is necessary to specify the type of distributions $\sigma(I)$ and $P_I(K)$ of the compound nuclei over I and K, respectively. If one assumes that the quantity $\sigma(I)$ is known, then the problem of angular distribution calculation consists only in the determination of the distribution $P_I(K)$, which could be found in the transition state. Two limiting assumptions on the location of the transition state are usually made; correspondingly, two versions of the transition-state theory exist: the saddle-point transition-state (SPTS) [61] and the scission-point transition-state (SCTS) [63] models. In the case of a multidimensional model, a set of relevant conditional saddle or scission points plays the role of transition states. In the SPTS and SCTS models an equilibrium distribution of K values is assumed; this is determined by the Boltzmann factor $\exp(-E_{\rm rot}/T)$ [64] at the saddle or scission point, respectively. Using Eq. (3) for the $E_{\rm rot}$ one can obtain the equilibrium K distribution

$$P^{\rm eq}_I(K) = \frac{\exp\left[-K^2/\left(2K_0^2\right)\right]}{\sum_{K=-I}^{I}\exp\left[-K^2/\left(2K_0^2\right)\right]}, \tag{10}$$

where the variance of the equilibrium K distribution is determined by the expression

$$K_0^2 = J_{\rm eff}T/\hbar^2. \tag{11}$$

Here T and $J_{\rm eff}$ are taken at the transition state.

One can also rewrite Eq. (9) for the case of the 4D dynamical calculations as

$$W(\theta) = \sum_{I=0}^{\infty} \sigma(I) \sum_{K=-I}^{I} P_I(K,t_{sc}) W(\theta,I,K), \qquad (12)$$

where $P_I(K,t_{sc})$ is the dynamical K distribution calculated from the 4D model at the scission surface for spin I. We will discuss this distribution later in Sec. III C.

The anisotropy of the fission-fragment angular distribution is then given by

$$A = \frac{W(0^0)}{W(90^0)}, \qquad (13)$$

where the angular distribution $W(\theta)$ could be found either from 4D calculations using Eq. (8) or from the equilibrium K distribution at the transition state using Eqs. (9)–(11).

Three quantities determine the angular distribution in the transition-state model: the initial spin distribution of the compound nuclei, the effective moment of inertia, and the nuclear temperature at the transition state. Note that the K distribution obtained from the 4D dynamical calculations will be identical to the equilibrium K distribution at a saddle point in case the relaxation time of the K degree of freedom, τ_K, is shorter than the time spent by the nucleus near the saddle point and larger than the time of descent from saddle to scission point. If, on the contrary, τ_K is much shorter than the descent time from saddle to scission point, the dynamically calculated K distribution will be similar to the equilibrium K distribution at the scission point. In the present dynamical calculations, we do not use any approximations for the K-coordinate relaxation time. Instead, we directly treat the relaxation process of the K coordinate using Eq. (2) and take into account the effect of the actual evolution of the K value on the dynamics of the shape parameters (q_1,q_2,q_3).

The analysis of the ensemble-averaged Eq. (2) leads to the expression for the K state relaxation time:

$$\frac{d\langle K\rangle}{dt} = -\frac{\gamma_K^2 I^2}{2}\left\langle \frac{\partial V}{\partial K}\right\rangle. \qquad (14)$$

From the expression for the rotational energy, it follows that

$$\frac{d\langle K\rangle}{dt} = -\frac{\gamma_K^2 I^2}{2}\frac{\hbar^2}{J_{\rm eff}}\langle K\rangle. \qquad (15)$$

By assuming a constant γ_K, as we do in the present study, the solution of this equation has the form

$$\langle K(t)\rangle_{K_0} = K_0 \exp\left[-\frac{\gamma_K^2 I^2 \hbar^2}{2J_{\rm eff}}(t-t_0)\right], \qquad (16)$$

which gives the following expression for the relaxation time:

$$\tau_K = \frac{2J_{\rm eff}}{\gamma_K^2 I^2 \hbar^2}. \qquad (17)$$

Another estimate for τ_K can be found in [65]:

$$\tau_K = \frac{C_K J_\perp^2}{[I(I+1)-K^2]\hbar^2}. \qquad (18)$$

It is based on the ideas of Randrup and Døssing [66]. Here, C_K is a coefficient that was varied to describe experimental data more precisely.

Concluding this section, we wish to stress that the dynamical treatment of the K-coordinate evolution by both the master equation for $P_I(K,t)$ [17–19] and the overdamped Langevin equation [13,14] introduces parameters: γ_K in the latter case and τ_K in the former case. As one can see from this section, these parameters are related to each other by Eq. (17). The values of γ_K and τ_K are deduced by fitting the observed anisotropy of the fission-fragment angular distribution.

III. RESULTS AND DISCUSSION

In the present study we have investigated several fusion-fission reactions, where the compound nuclei from ^{105}Ag to ^{260}Rf were formed:

^{93}Nb + ^{12}C → ^{105}Ag($E_{\rm lab}$ = 1060 MeV);
^{18}O + ^{144}Sm → ^{162}Yb($E_{\rm lab}$ = 158.8 MeV);
^{18}O + ^{154}Sm → ^{172}Yb($E_{\rm lab}$ = 158.8 MeV);
^{16}O + ^{184}Pt → ^{200}Pb($E_{\rm lab}$ = 91.6,97.7,102.5, and 107.9 MeV);
^{18}O + ^{197}Au → ^{215}Fr($E_{\rm lab}$ = 158.4 MeV);
^{16}O + ^{208}Pb → ^{224}Th($E_{\rm lab}$ = 108 MeV);
^{16}O + ^{232}Th → ^{248}Cf($E_{\rm lab}$ = 128 MeV);
^{16}O + ^{238}U → ^{254}Fm($E_{\rm lab}$ = 90,96,110,114,130,140,148, 215, and 250 MeV);
^{16}O + ^{248}Cm → ^{264}Rf($E_{\rm lab}$ = 110,130, and 148 MeV);
^{20}Ne + ^{240}Pu → ^{260}Rf($E_{\rm lab}$ = 142 and 174 MeV);
^{18}O + ^{246}Cm → ^{264}Rf($E_{\rm lab}$ = 102.5 MeV);
^{18}O + ^{238}U → ^{256}Fm($E_{\rm lab}$ = 159 MeV).

Some of these reactions have been considered in our previous studies performed with the 3D Langevin model [20,21], so the influence of the K coordinate on calculated observables can be examined. We also present some recent results of 4D calculations [15] in order to have more complete data for comparison between the 3D and 4D Langevin calculations. The 3D and 4D Langevin calculations provide large amount of observables. Some of them are brought together with the experimental data in Table I. The following sections describe the comparison of calculated results and available experimental data.

A. Fission rate, time, probability, and prescission neutron multiplicity

Our previous investigation [74] has shown that the inclusion of new collective shape coordinates in dynamical modeling results in an increase of the stationary value of the fission rate in multidimensional Langevin calculations. In the present study we investigate in detail the influence of the K coordinate on a fission rate and time characteristics and how the inclusion

TABLE I. Calculated results for the fission of ^{105}Ag, ^{172}Yb, ^{162}Yb, ^{215}Fr, ^{224}Th, ^{248}Cf, ^{256}Fm, ^{260}Rf, and ^{264}Rf together with the available experimental data. The 4D calculations were performed with $\gamma_K = 0.077$ (MeV zs)$^{-1/2}$. The columns list (from left to right) the compound nucleus (CN), Z^2/A, the excitation energy (E^*), the reduction coefficient k_s, the variance of the fission fragment mass (σ_M^2) and kinetic energy ($\sigma_{E_K}^2$) distributions, the mean total kinetic energy ($\langle E_K \rangle$), the mean multiplicity of prescission neutrons ($\langle n_{\rm pre} \rangle$), the mean descent time from saddle to scission point ($\langle \tau_{\rm sd-sc} \rangle$), the mean time spent by the fissioning system near the saddle point ($\langle \tau_{\rm sd} \rangle$), and the mean time to reach the saddle point ($\langle \tau_{\rm gs-sd} \rangle$).

CN	Z^2/A	E^* (MeV)	k_s	σ_M^2 (u^2)	$\sigma_{E_K}^2$ (MeV^2)	$\langle E_K \rangle$ (MeV)	$\langle n_{\rm pre} \rangle$	$\langle \tau_{\rm sd-sc} \rangle$ (zs)	$\langle \tau_{\rm sd} \rangle$ (zs)	$\langle \tau_{\rm gs-sd} \rangle$ (zs)
^{105}Ag	21.04	121	0.25	233 ± 22	41 ± 4	58.5 ± 0.2	1.36	0.08	8.1	36
			$k_s(q_1)$	250 ± 17	42 ± 3	58.1 ± 0.2	1.37	0.09	7.8	44
			1.0	229 ± 23	40 ± 3	58.2 ± 0.2	1.79	0.1	8.0	52
exp. [67]				219		69 ± 3	1.5			
^{172}Yb	28.49	128	0.25	271 ± 8	82 ± 3	$114. \pm 0.1$	4.64	3.75	4.47	84
			$k_s(q_1)$	254 ± 8	89 ± 3	113.5 ± 0.1	4.91	4.22	10.81	165
			1.0	230 ± 11	73 ± 4	113.7 ± 0.1	5.33	4.35	10.64	183
exp. [68]				228	112	113	4.4 ± 0.15			
^{162}Yb	30.25	118	0.25	292 ± 7	123 ± 3	114.9 ± 0.1	2.84	2.46	4.41	66
			$k_s(q_1)$	280 ± 7	116 ± 3	114.5 ± 0.1	3.03	3.38	7.16	111
			1.0	245 ± 6	111 ± 3	115 ± 0.1	3.5	4.16	10.01	179
exp. [68]				231		112	2.45 ± 0.25			
^{215}Fr	35.20	113	0.25	385 ± 11	138 ± 4	160.4 ± 0.1	4.26	4.79	8.3	65
			$k_s(q_1)$	346 ± 10	137 ± 4	160.4 ± 0.1	4.56	5.38	7.16	111
			1.0	298 ± 10	135 ± 4	160.8 ± 0.1	5.35	8.91	22.28	133
exp. [68]				272	190	154	4.1 ± 0.15			
^{224}Th	36.16	54	0.25	308 ± 5	94 ± 2	169.5 ± 0.1	2.13	7.88	23.28	128
			$k_s(q_1)$	271 ± 4	85 ± 2	168.5 ± 0.1	2.31	11.17	39.2	132
			1.0	241 ± 5	79 ± 2	168.2 ± 0.1	2.86	12.24	41.33	241
exp. [69,70]				213	137	162.4 ± 1	2.5			
^{248}Cf	38.73	83	0.25	519 ± 7	184 ± 3	198.3 ± 0.1	2.65	2.81	7.56	28
			$k_s(q_1)$	458 ± 6	165 ± 3	191.4 ± 0.1	2.81	4.18	11.88	23
			1.0	355 ± 12	130 ± 4	191.3 ± 0.1	4.11	7.53	43.42	102
exp. [71]				456 ± 18	311 ± 22	184	4.1			
^{256}Fm	39.06	159	0.25	615 ± 17	233 ± 7	197.2 ± 0.2	3.85	2.13	3.51	24
			$k_s(q_1)$	550 ± 15	204 ± 6	197.1 ± 0.2	4.08	3.0	5.17	20
			1.0	415 ± 12	161 ± 5	197.8 ± 0.2	5.62	4.63	17.04	79
exp. [68]				543	420	181.0	5.1			
^{260}Rf	41.6	75	0.25	626 ± 9	266 ± 4	211.6 ± 0.1	1.47	1.7	3.08	18
			$k_s(q_1)$	562 ± 8	236 ± 4	211.7 ± 0.1	1.63	2.44	4.17	15
			1.0	458 ± 7	193 ± 3	211.9 ± 0.1	2.72	3.7	14.87	62
exp. [72]				506 ± 12	372 ± 13	195 ± 2	3.5			
^{260}Rf	41.6	105	0.25	685 ± 10	305 ± 4	211.5 ± 0.1	2.82	1.63	2.9	17
			$k_s(q_1)$	623 ± 9	271 ± 4	211.7 ± 0.1	3.02	2.31	3.95	13
			1.0	486 ± 7	206 ± 3	212.4 ± 0.1	4.57	3.48	14.56	57
exp. [72]				620 ± 17	424 ± 15	196 ± 2	5.7			
^{264}Rf	40.97	52	0.25	568 ± 8	218 ± 3	210.6 ± 0.1	0.90	2.1	4.64	21
			$k_s(q_1)$	503 ± 7	194 ± 3	210.4 ± 0.1	1.02	3.03	6.3	16
			1.0	421 ± 6	170 ± 3	210.7 ± 0.1	1.83	5.09	24.34	70
exp. [69,73]				435		198	2.0			

of the K coordinate in the dynamical consideration will influence the fission observables such as prescission neutron multiplicity and fission probability. In a previous study [15] we demonstrated that the values $k_s = 0.25$ and $\gamma_K \simeq 0.077$ (MeV zs)$^{-1/2}$ provide a good description of the experimental MED characteristics and the anisotropy of the fission-fragment angular distribution for the ^{224}Th and ^{248}Cf compound nuclei in a wide interval of excitation energy. It was also found that the dissipation coefficient γ_K influences only the angular distribution of fission fragments and practically has no effect on the prescission particles multiplicity, fusion-fission and evaporation residue cross sections, and fission-fragment MED parameters.

In the present study we demonstrate the influence of the K coordinate on the fission time distribution and fission rate in Figs. 3 and 4. In Fig. 3 the fission rates calculated in the 3D and 4D models are presented for different nuclei. These calculations were performed to distinguish only the

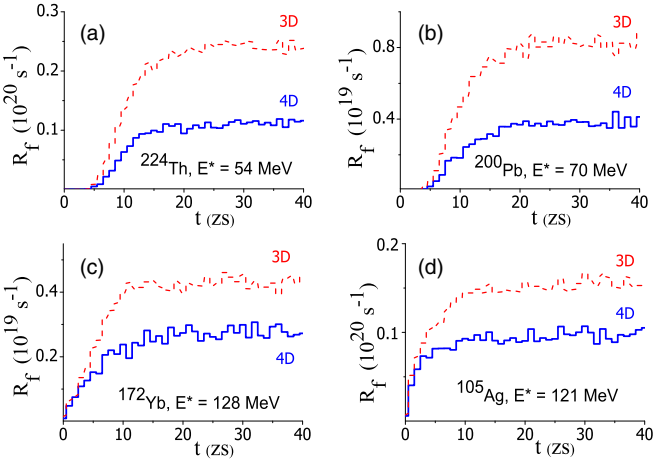

FIG. 3. (Color online) The fission rate for ^{224}Th (a), ^{200}Pb (b), ^{172}Yb (c), and ^{105}Ag (d) in calculations with the 3D (dashed histogram) and 4D (solid histogram) dynamical models. The calculations were performed at fixed spin $I = 40$ and without taking into account the evaporation of prescission particles.

influence of the K coordinate on R_f; therefore, the evaporation of the prescission particles were switched off and calculations were performed with the fixed value of angular momentum $I = 40$. The present calculations show that inclusion of the K coordinate in the dynamical consideration results in a decrease of fission rate. This decrease is around 50% for heavy (^{224}Th and ^{200}Pb) and 30% for light (^{172}Yb and ^{105}Ag) nuclei. In the dynamical calculations with lower dimensionality the inclusion of the K coordinate will result in an approximately the same decrease of the fission rate. These results support the findings [13,14] that a proper account of nonzero K values is needed in the expression for the calculations of stationary fission width. This could be particularly important for the elucidation of the energy dependence of nuclear viscosity on excitation energy [13,14]. It should be noted also that the K coordinate will change the potential energy surface near the ground state and saddle points, which could be accounted for in the Kramers-like expression for the stationary value of the fission decay width [75] as well.

The fission rate $R_f(t)$ has a direct correlation with the fission time distribution, which is presented in Fig. 4 for the ^{224}Th and ^{248}Cf compound nuclei. The delay time τ_d determines the time interval $0 < t < \tau_d$ where no fission events occur, and $\tau_d = 3$ zs is found for both ^{224}Th and ^{248}Cf nuclei in 3D and 4D calculations. The steep rise of the fission time distribution corresponds to the increase of $R_f(t)$ to the stationary value at $t_{\max}$. For time interval $t > t_{\max}$ the exponential decrease of the fission time distribution corresponds to a constant value of $R_f(t)$ with a long-lasting tail up to 10^{-18} s, which is influenced by the evaporation of prescission light particles. The $t_{\max}$ value is affected very little by the dimensionality of the dynamical model. On the other hand, the incline of the tail is the characteristic mostly affected by the dimensionality. As a result, the mean fission time $\langle t_f \rangle$ demonstrates the strongest sensitivity to the inclusion of the K coordinate. The different incline of time distribution tails

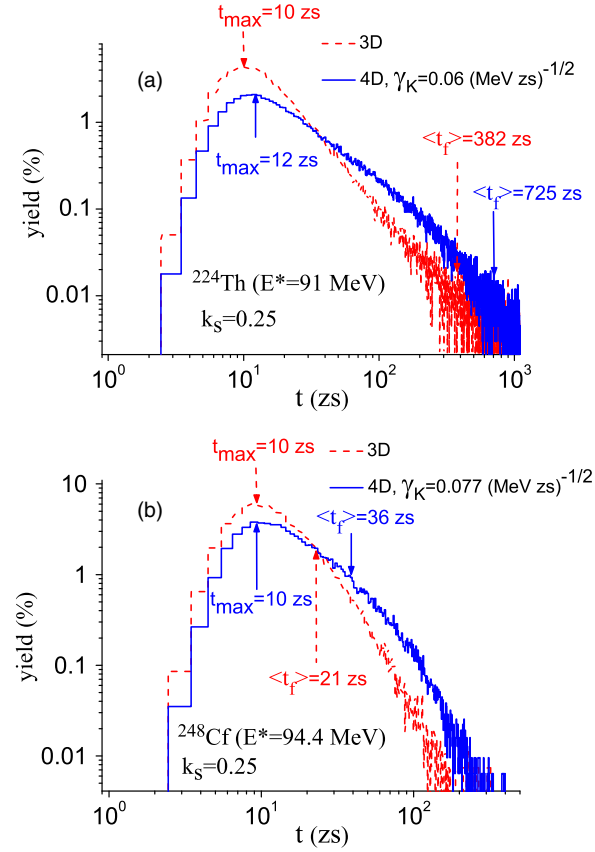

FIG. 4. (Color online) The fission time distribution for the ^{224}Th (a) and ^{248}Cf (b) fissioning nuclei in the 3D (dashed histogram) and 4D (solid histogram) calculations obtained with $k_s = 0.25$ and different γ_K values.

in the 3D and 4D calculations in Fig. 4 is the reflection of the fission rate decrease in the 4D calculations in comparison with the 3D ones. In our previous study [15] we have found that this decrease is caused by the appearance of an additional conservative force slowing down the motion in the fission direction and the increase of the fission barrier height after the inclusion of the nonzero K values in the dynamical consideration.

In spite of the fact that direct fission time measurements are possible at the present time [76], such data are quite rare and the experimental uncertainty is large. Therefore, the fission probability and prescission neutron multiplicity, which are directly connected with a fission rate and fission time characteristics, are compared widely with the experimental data. The number of prescission particles emitted during a fission process could be associated with the fission time scale [77] and easily available for the experimental and theoretical studies. The prescission particles carry away the excitation energy and spin. Therefore, they influence the other observables determined by the compound nucleus temperature such as variances of fission fragments mass and kinetic energy distributions and the fission probability. In the present study we mainly deal with the reactions where experimental data on the prescission neutron multiplicity are available. Thus, we

concentrate on the analysis of the mean prescission neutron multiplicity $\langle n_{\rm pre}\rangle$.

We performed calculations for several heavy fissioning systems, where the 3D Langevin calculations [20,21] fail to reproduce simultaneously the prescission neutron multiplicities and the width of fission-fragment mass and kinetic energy distributions. Reproduction of MED parameters in the 3D calculations required small values of $k_s \simeq 0.1$, whereas $k_s \geqslant 1$ values are needed to reproduce prescission neutron multiplicities [20]. In the 4D calculations the consistent description of MED parameters and $\langle n_{\rm pre}\rangle$ could be obtained with much closer k_s values. We obtain around a 10% increase of $\langle n_{\rm pre}\rangle$ and at the same time around an 80% increase of σ_M^2 as a result of the dynamical calculations with nonzero K values, which increase fission barrier heights and decrease the stiffness of the nucleus with respect to mass-asymmetry deformations. Thus, for very heavy nuclei $Z^2/A > 38$ the experimental $\langle n_{\rm pre}\rangle$ values could be reproduced with k_s around 1.0, or with deformation-dependent $k_s(q_1)$. At the same time these large k_s values also allow for a wider mass distribution. For lighter nuclei $35 < Z^2/A < 38$ the experimental $\langle n_{\rm pre}\rangle$ values could already be reproduced with $k_s(q_1)$. Such k_s values allow one to obtain a variance of the mass distribution, σ_M^2, in the calculations, which is close to the experimental one (with the difference between experimental and calculated σ_M^2 values not exceeding 30%). Considering the deformation-dependent $k_s(q_1)$ obtained from the chaos-weighted wall formula one can see that these calculations predict larger $\langle n_{\rm pre}\rangle$ values compared to that with $k_s = 0.25$. This is due to the enhanced emission during the descent from saddle to scission point, where $k_s(q_1) > 0.25$.

For the lighter systems the mean prescission neutron multiplicity could be reproduced with lower k_s values. The calculations with $k_s = 0.25$ are already very close to the experimental data. At the same time the calculated σ_M^2 values exceed the experimental data by about 20%, and the best reproduction of σ_M^2 could be obtained with $k_s = 1$. Thus, the calculations with $k_s(q_1)$ provide a reasonable balance, ensuring satisfactory reproduction of both σ_M^2 and $\langle n_{\rm pre}\rangle$ experimental values with reasonable quality. More subtle tuning of the parameters of the statistical model [78] that governs particle evaporation, for example, the level-density parameter a, could also provide better reproduction of prescission particle multiplicities.

The reactions with the compound nucleus ^{200}Pb were investigated in detail in the present study. The preliminary results of our investigations were presented in Ref. [81], where we tried to extract nuclear viscosity for the shape coordinates (k_s values) and γ_K from $\langle n_{\rm pre}\rangle$ and the anisotropy of the fission-fragment angular distribution. In the present study, we add the fission probability (P_f) to the analysis in order to make more reliable conclusions. Therefore, we found a combination of k_s and γ_K that better describes $\langle n_{\rm pre}\rangle$, P_f, and the anisotropy of the fission-fragment angular distribution. The comparison between the calculated results and experimental data on $\langle n_{\rm pre}\rangle$ and P_f is presented in Fig. 5. The results and discussion on the anisotropy of the fission-fragment angular distribution are presented in Sec. III C. The good reproduction of the experimental values of $\langle n_{\rm pre}\rangle$ and P_f for ^{200}Pb could be obtained with $k_s = 0.3$ or $k_s(q_1)$. The coefficient γ_K does not influence these observables. At the same time the anisotropy of the fission-fragment angular distribution is determined by both k_s and γ_K parameters [15]. Thus, as will be shown in Sec. III C, $\gamma_K \simeq 0.2$ (MeV zs)$^{-1/2}$ is needed to reproduce the anisotropy of the fission-fragment angular distribution with k_s around 0.3 or $k_s(q_1)$.

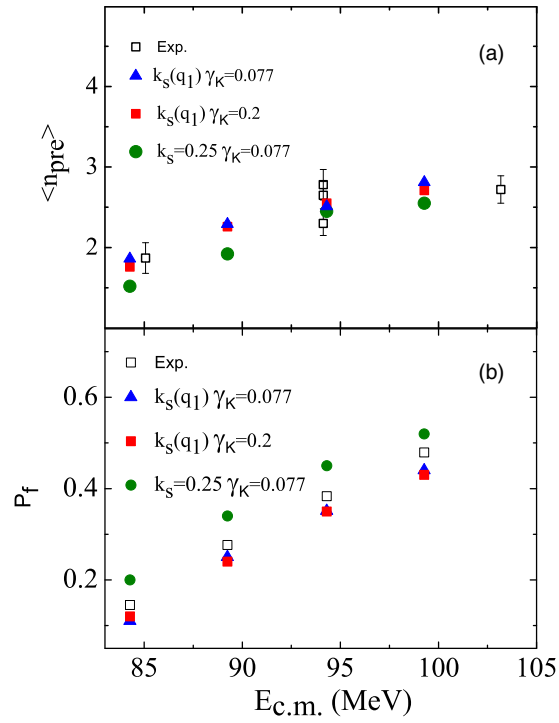

FIG. 5. (Color online) The prescission neutron multiplicity (a) and fission probability (b) for the compound nucleus ^{200}Pb as a function of center-of-mass energy. The open squares are experimental data from Refs. [79,80]. The filled symbols are the calculated results with $k_s = 0.25$ and $\gamma_K = 0.077$ (MeV zs)$^{-1/2}$ (circles), with the chaos-weighted wall formula $k_s(q_1)$ and $\gamma_K = 0.077$ (MeV zs)$^{-1/2}$ (triangles), and with the chaos-weighted wall formula $k_s(q_1)$ and $\gamma_K = 0.2$ (MeV zs)$^{-1/2}$ (squares).

B. Parameters of the MED of fission fragments

Mass-energy distributions of fission fragments are traditionally used as one of the main sources of information about the dynamics of the fission process and about the mechanism that governs the separation of a nucleus into fragments. Systematic experimental and theoretical investigations of the MED were pioneered in the classic studies of Plasil and co-authors [82] and Nix and Swiatecki [83,84].

Extensive experimental investigations devoted to exploring the MED and the fission-fragment angular distribution yielded a vast body of important information. The majority of those experimental studies were systematized and analyzed in [68,69,72,80,85–90]. In the theory, considerable advances in describing special features of the fission-fragment MED and in obtaining deeper insight into the role of nuclear dissipation were made within the diffusion model based on the multidimensional Fokker-Planck equation for the distribution of collectives variables [91–93]. Further

development of the stochastic approach to fission dynamics on the basis of the 3D Langevin equations [2,11,20,43] makes it possible to perform a comprehensive study of the fission-fragment MED and multiplicities of prescission particles. The results of this systematic investigation were published in [2,20,21,43].

The contour plots of isolines for the distribution $Y(E_K,M)$, where E_K is the total kinetic energy and M is the mass of the fission fragment, is the clearest and most comprehensive way to represent the fission-fragment MED. These plots are of interest since they provide the possibility of studying correlations between the parameters of the distribution and of performing a comparison with experimental data. The method that we employ to calculate the two-dimensional MED of fission fragments relies on the concept of a scission surface. We assume that, as soon as a stochastic Langevin trajectory crosses the scission surface, there occurs an instantaneous rupture of the neck without changes in the elongation of the nucleus and in the mass asymmetry. In the case being considered, the instantaneousness means that the rupture of the neck occurs within a time much shorter than the time of descent from a saddle to scission point. The MED calculation method is described in detail in our previous publications [43,94]. The explicit formulas for the fragment mass and total kinetic energy of fragments, E_K, in terms of collective coordinates $\mathbf{q_{sc}}$, conjugate momenta $\mathbf{p_{sc}}$ at the scission surface, and the profile function $\rho_s(z,\mathbf{q_{sc}})$ can be found in Refs. [2,20,21,43,94].

Figure 6 shows the contour isolines of the fission-fragment MED $Y(E_K,M)$ for three compound nuclei. From this figure, one can see that the shapes of the contour plots are close to ellipsoidal in the region of large values of $Y(E_K,M)$ and are similar to triangles in the region of small values of $Y(E_K,M)$. The similar shapes of the contour plots were observed in the experimental study reported in [72].

In order to perform a quantitative comparison and estimations, it is necessary to consider the one-dimensional mass and energy distributions by integrating the two-dimensional distribution $Y(E_K,M)$ with respect to a corresponding parameter (E_K in the case of a mass distribution and M in the case of an energy distribution). The mass and energy distributions have a one-humped shape (similar to the shape of a Gaussian distribution) for all nuclei considered here, with the exception of ^{105}Ag, for which we obtained a uniform distribution, as this nucleus is close to the Businaro-Gallone point.

The calculated parameters of the fission-fragment kinetic energy distribution, $\sigma^2_{E_K}$ and $\langle E_K\rangle$, are compared with the experimental data in Table I. The qualitative dependence of $\sigma^2_{E_K}$ and $\langle E_K\rangle$ on the dissipation coefficient k_s in 4D calculations is the same as in the previous 3D calculations [2,20,21]. The experimental $\sigma^2_{E_K}$ are underestimated in the dynamical calculations. We have already discussed [2,15,95,96] that the main reason for this underestimation is the insufficient flexibility of the (c,h,α) parametrization, which cannot generate the elongated shapes with a thick and long cylindrical neck. The calculated $\langle E_K\rangle$ values in the 4D calculations for the heaviest nuclei considered in the present study are around 12–16 MeV larger than the experimental values. The agreement becomes better for lighter nuclei with $Z^2/A < 39$.

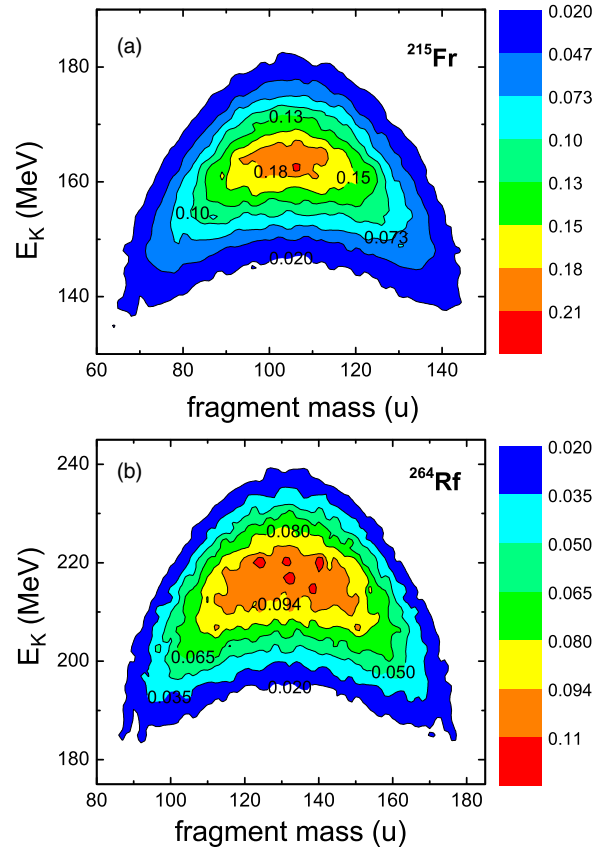

FIG. 6. (Color online) The fission fragment MED of ^{215}Fr (a) and ^{264}Rf (b) obtained from 4D calculations with the chaos-weighted wall formula $k_s(q_1)$. The numbers at the contour lines in percent indicate the yield, which is normalized to 200%.

The growth of the variance of the mass distribution with the parameter Z^2/A could be reproduced for heavy compound nuclei $Z^2/A > 36$ with deformation-dependent $k_s(q_1)$. Agreement with experimental data is not only qualitative but also quantitative (the deviation from experimental data being less than 30%). For lighter nuclei the $k_s(q_1)$ found on the basis of the chaos-weighted wall formula also provides values of σ^2_M and $\langle n_{\rm pre}\rangle$ close to those of the experimental data. For the reaction leading to the production of the compound nucleus ^{105}Ag, the fission-fragment mass distribution is close to uniform. In Fig. 7 the comparison between theoretical calculations and experimental data on the fission-fragment charge distribution is presented. The theoretical fission-fragment charge distribution for ^{105}Ag was obtained from the mass distribution under the assumption of a uniform charge distribution between fission fragments proportional to their masses. As one can see from Fig. 7, the 4D theoretical calculations could reproduce sufficiently well the shape and yield of the experimental charge distribution in the range of fission-fragment charge (mass) $10 < Z < 35$ ($20 < M < 80$), where the contribution from the fusion-fission mechanism is most prominent. In Table I we present the σ^2_M estimation for ^{105}Ag for the same limits of fission-fragment masses.

In [2,21], the calculations of σ^2_M were performed on the basis of the 3D model ($K = 0$). Those calculations revealed

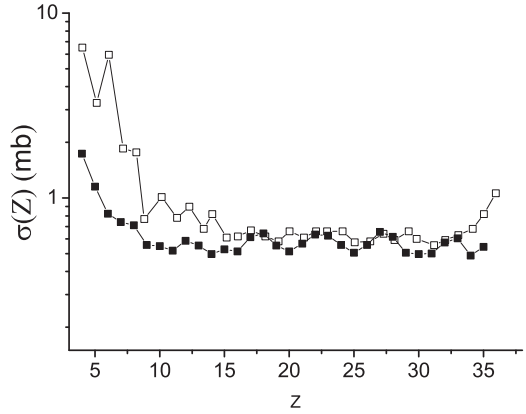

FIG. 7. The charge distribution for the reaction ^{93}Nb + ^{12}C → ^{105}Ag ($E_{\rm lab}$ = 1060 MeV). The open squares are experimental data [67] and filled squares are results of 4D calculations with the chaos-weighted wall formula $k_s(q_1)$.

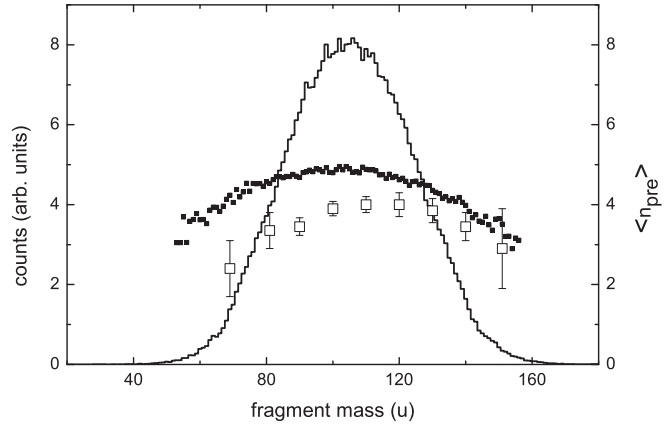

FIG. 9. The mass distribution of fission fragments (solid histogram) measured in coincidence with the prescission neutron multiplicities $\langle n_{\rm pre}(M)\rangle$ (open squares) compared with the theoretical 4D calculations for the reaction ^{18}O + ^{197}Au → ^{215}Fr at $E_{\rm lab}$ = 158.4 MeV. Theoretical calculations were performed with the chaos-weighted wall formula $k_s(q_1)$.

that the 3D model describes well the mass distributions of heavy nuclei at $k_s = 0.1$–0.25. From our present calculations, it follows that the inclusion of the K coordinate allows us to keep the good description of σ_M^2 values at larger k_s, which will allow us to reproduce $\langle n_{\rm pre}\rangle$ for heavy nuclei. The effect of an increase of σ_M^2 for heavy nuclei upon going over from the 3D to the 4D model is due to a decrease in the stiffness of the fissile nucleus with respect to the mass-asymmetric deformation. Figure 8 demonstrates the dependence of the stiffness $\partial^2 F/\partial\eta^2$, over the descent from the saddle to the scission point, where $\eta = 2(M_L - M_R)/A_{\rm CN}$ is the mass-asymmetry coordinate, which is frequently used in analyzing relevant experimental data [72,89,90], and M_L and M_R are the masses of the fission fragments.

As an important test of the present 4D model we performed calculations of $\langle n_{\rm pre}(M)\rangle$ and $\langle n_{\rm pre}(E_K)\rangle$ dependencies. These dependencies were studied experimentally

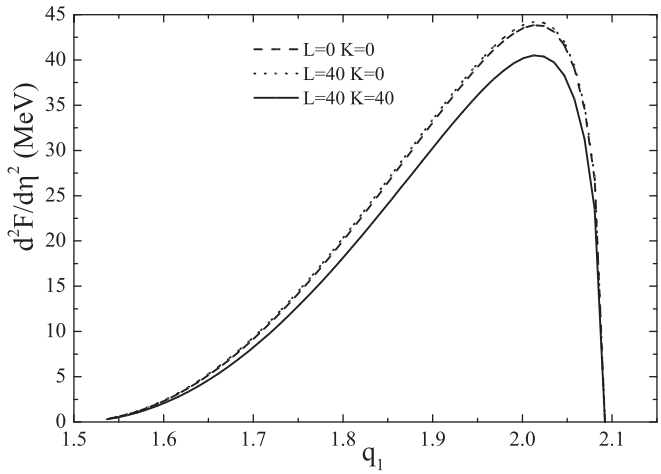

FIG. 8. The stiffness for ^{260}Rf with respect to the mass-asymmetry coordinate η along the bottom of the fission valley as a function of the elongation parameter q_1. Different combinations of I and K are considered as indicated.

[68] and theoretically [21] using the 3D Langevin model. It was shown [68] that for many fusion-fission reactions the number of evaporated neutrons is larger for symmetric than for asymmetric mass splitting. It was found that the dependence $\langle n_{\rm pre}(M)\rangle$ can be approximated by a parabolic function

$$\langle n_{\rm pre}(M)\rangle = \langle n_s\rangle - c_{\rm pre}\,(M_s - M)^2\,, \qquad (19)$$

where $\langle n_s\rangle$ is the mean value of the prescission neutron multiplicity for symmetric fission, M_s is the fragment mass for symmetric fission, and $c_{\rm pre}$ is a variable parameter. From the experimental data, it was found in [68] that $c_{\rm pre}$ = 14± 1 and 6.5 ± 0.5 for the reaction ^{18}O + ^{154}Sm → ^{172}Yb at $E_{\rm lab}$ = 158.3 MeV and the reaction ^{18}O + ^{197}Au → ^{215}Fr at $E_{\rm lab}$ = 158.4 MeV, respectively. Our theoretical calculations performed at k_s = 0.25 yielded $c_{\rm pre}$ = 13.9 ± 0.2 and 6.1 ± 0.2 for these reactions. In case of $k_s(q_1)$ $c_{\rm pre}$ = 8.1 ± 0.9 and 6.8 ± 0.1 were found from the 4D calculations. These results are in good agreement with experimental data and close to the previous results of the 3D calculations [21]. An example of the dependence $\langle n_{\rm pre}(M)\rangle$ is given in Fig. 9 together with the fission-fragment mass distribution. In Fig. 10 we present the fission-fragment kinetic energy distribution with the dependence $\langle n_{\rm pre}(E_K)\rangle$ obtained in the 4D calculations with $k_s(q_1)$. A detailed discussion of the reasons for the parabolic dependence of $\langle n_{\rm pre}(M)\rangle$ and approximate independence $\langle n_{\rm pre}\rangle$ of E_K can be found in Ref. [21]. The inclusion of the K coordinate in the dynamical consideration and introduction of the deformation-dependent $k_s(q_1)$ does not change qualitatively the mechanisms that govern the formation of correlation dependencies $\langle n_{\rm pre}(M)\rangle$ and $\langle n_{\rm pre}(E_K)\rangle$.

C. Angular distribution of fission fragments

Early stages of the investigation of fission fragment angular distributions involved an analysis of the reactions induced by neutrons, ^{3}He ions, and α-particle projectiles. The compound nuclei produced in such reactions have a temperature of about

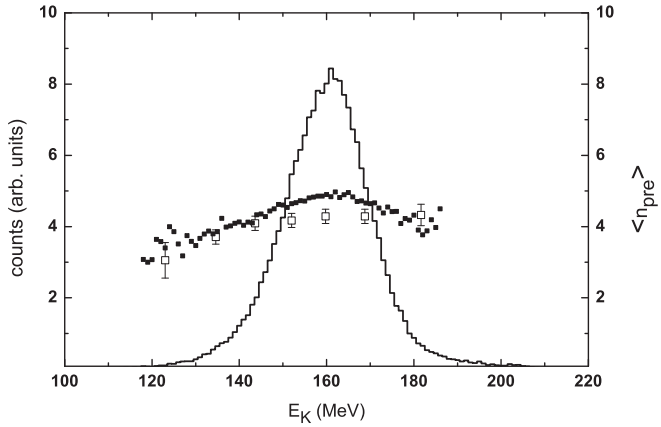

FIG. 10. The kinetic energy distribution of fission fragments (solid histogram) measured in coincidence with the prescission neutron multiplicities $\langle n_{\rm pre}(E_K)\rangle$ (open squares) compared with the theoretical 4D calculations for the reaction $^{18}\mathrm{O} + {}^{197}\mathrm{Au} \rightarrow {}^{215}\mathrm{Fr}$ at $E_{\rm lab} = 158.4$ MeV. Theoretical calculations were performed with the chaos-weighted wall formula $k_s(q_1)$.

1 MeV and low values of angular momentum. For these reactions, usually the fission barrier height is much greater than the nuclear temperature and the SPTS model provides fairly good reproduction of the experimental data on the anisotropy of the fission-fragment angular distribution.

A further investigation of the fission-fragment angular distribution was performed with heavier projectiles, such as massive ions of carbon and oxygen and ions with larger masses. It became possible to study angular distributions of fission fragments in the fission of heavy compound nuclei that have much higher temperatures and angular momenta. In the early 1980s it was found experimentally [97–99] that in these reactions the angular anisotropy in a heavy-ion-induced fission could differ a lot from the predictions of the SPTS model. In order to overcome the above difficulties the SCTS model was proposed in [97,98,100,101]. Instead of the saddle point, the more deformed scission point was taken as an effective transition state. A physical explanation of this displacement can be found in the transformation [85,102,103] of the landscape of the potential energy surface of a compound nucleus with increasing angular momentum. The increasing angular momentum I leads to a shift of the saddle point [85,102,103] to smaller deformation, while the fission barrier decreases. This means that the fission process at high values of I leads to a long descent from saddle to scission point. If the time of descent from the saddle to the scission point is sufficiently long the tilting mode may become unfrozen, so that the formation of angular distributions of fragments occurs at the scission point in the limiting case. This assumption forms a basis for the theoretical SCTS models developed in [97,98,100,101].

At the same time, it was shown [104] that sometimes the experimentally observed angular distribution anisotropy cannot be described by either the SPTS or SCTS models. Therefore, it could be assumed, in the general case, that the transition state is located somewhere between the saddle and scission points. The existing uncertainty with the position

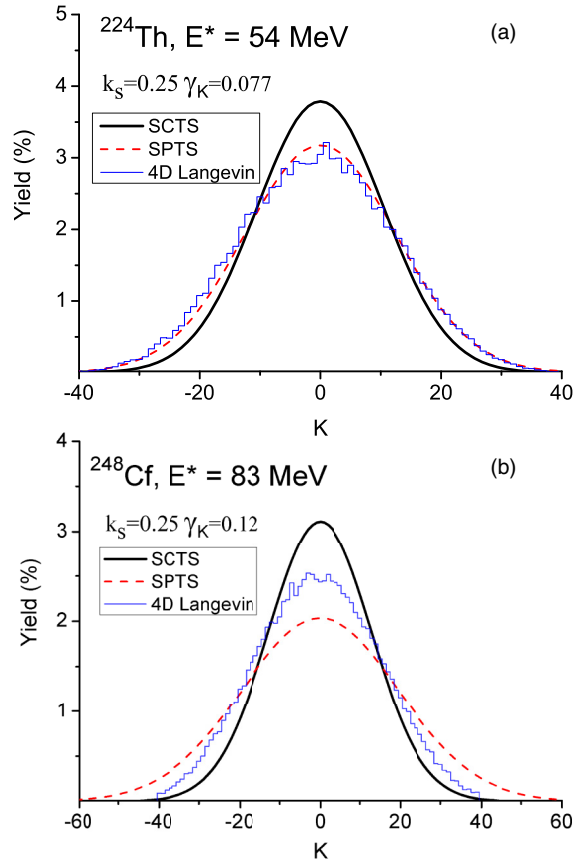

FIG. 11. (Color online) The non equilibrium K distribution of the fissioning nuclei ^{224}Th (a) and ^{248}Cf (b) at the scission surface $P_I(K,t_{\rm sc})$. The distributions $P_I(K,t_{\rm sc})$ obtained from the 4D calculations are shown by the thin solid histograms. The 4D Langevin calculations for the ^{224}Th and ^{248}Cf nuclei were performed with $k_s = 0.25$ and $\gamma_K = 0.077\,(\mathrm{MeV\,zs})^{-1/2}$, and with $k_s = 0.25$ and $\gamma_K = 0.12\,(\mathrm{MeV\,zs})^{-1/2}$, respectively. The equilibrium K distributions $P_I^{\rm eq}(K)$ obtained from SCTS and SPTS models are shown by the solid and dashed curve, respectively. The calculations were performed with the value of angular momentum $I = 40$.

of the transition state indicates that it is necessary to take into account [16–19] the dynamical features of the angular distribution formation. In this case the tilting mode could be considered as an independent collective coordinate in the multidimensional Langevin dynamics. Such a completely dynamical approach makes it possible to determine in the most general form the nonequilibrium K-mode distribution $P_I(K,t)$. Figure 11 shows the K distributions $P_I(K,t_{\rm sc})$ at the scission surface that were calculated dynamically within the 4D Langevin approach for the ^{224}Th and ^{248}Cf compound nuclei. The K distributions obtained within the SPTS and SCTS models are also presented in this figure. One can see from this figure the influence of the γ_K parameter on the equilibration of the K coordinate.

The observable that is directly determined by the dynamical evolution of the K coordinate is the angular distribution of fission fragments. The present and our recent 4D calculations [15] demonstrate that both parameters k_s and γ_K influence the

fission-fragment angular distribution. In our previous study [15] we examined the angular distribution formation for the compound nuclei ^{224}Th and ^{248}Cf. In the present paper the 4D calculations were performed for the reactions $^{16}\mathrm{O} + {}^{184}\mathrm{Pt} \rightarrow {}^{200}\mathrm{Pb}$, $^{16}\mathrm{O} + {}^{238}\mathrm{U} \rightarrow {}^{254}\mathrm{Fm}$, and $^{18}\mathrm{O} + {}^{246}\mathrm{Cm} \rightarrow {}^{264}\mathrm{Rf}$. The anisotropies of the fission fragment angular distributions are presented in Fig. 12. We have chosen the last two reactions because neither the SPTS nor the SCTS model can describe the full set of experimental data [18,19].

It is seen from the results of the 4D calculations that the deformation-dependent $k_s(q_1)$ and the value $\gamma_K \simeq 0.077$ $(\mathrm{MeV\,zs})^{-1/2}$ for $A_{\mathrm{CN}} > 220$ and $\gamma_K \simeq 0.2(\mathrm{MeV\,zs})^{-1/2}$ for A_{CN} around 200 describes fairly well the experimental data on the anisotropy of the angular distribution of fission fragments. It is clearly seen from the figures that the dynamical calculations for heavy nuclei give results closer to the predictions of the SPTS model than to the predictions of the SCTS model. This can be interpreted as a consequence of the relations of the characteristic times $\tau_{\mathrm{gs-sd}}$, τ_{sd}, and $\tau_{\mathrm{sd-sc}}$. Typical values of these times for different nuclei could be found in Table I. In our previous study [15] the relaxation time of the tilting mode, $\tau_K \sim 10$ zs, was estimated and shown to have a strong dependence on the spin, the deformation, and γ_K. For the heavy fissioning nuclei the relaxation time of the tilting mode, τ_K, is larger than $\langle\tau_{\mathrm{sd-sc}}\rangle$. Therefore, one could not expect that the equilibrium distribution of the tilting mode is reached at scission configuration. On the other hand, τ_K is comparable with $\langle\tau_{\mathrm{gs-sd}}\rangle$ and $\langle\tau_{\mathrm{sd}}\rangle$. Therefore, memory of the former distribution of the tilting mode at the saddle point and even at deformations before the saddle point can determine the resulting fission-fragment angular distribution at scission. For the light nuclei, the saddle and scission points are close to each other. Moreover, the inclusion of the K coordinate in the calculation of potential energy shifts the saddle point toward scission deformation [15]. Thus, the SPTS and SCTS models predict quite close results for light nuclei. Therefore, we present in Fig. 12 only the results of the anisotropy calculations performed with the SPTS model and 4D dynamical calculations for the ^{200}Pb nucleus. The mean descent time $\langle\tau_{\mathrm{sd-sc}}\rangle$ for light nuclei is less than 10 zs, and the mean time to reach saddle point deformations $\langle\tau_{\mathrm{gs-sd}}\rangle$ is usually comparable or larger than 100 zs. Therefore, the pre-saddle history of dynamical evolution of the fissioning systems can substantially influence the fission observables.

It should be noted that the earlier obtained estimates of τ_K lie in a rather wide interval from 5–8 zs [105–108] to 60 zs [109]. We stress that the relaxation time $\tau_K = 5$–6 zs was determined in [105] within a one-dimensional Langevin model, while, in other studies, calculations were performed within statistical models. At the same time, it follows from [54,66] that there is a dependence of τ_K on the velocity of nuclear rotation; i.e., considering the tilting mode relaxation time as a constant is only an approximation. Only recently [65,110,111] have the first dynamical calculations been carried out using the dependence of τ_K (or γ_K) on the velocity of the nuclear rotation. However, in the framework of a statistical model these results of Døssing and Randrup [54,55] have been applied earlier to the analysis of the angular distribution of fission fragments [112]. The authors of this study achieved

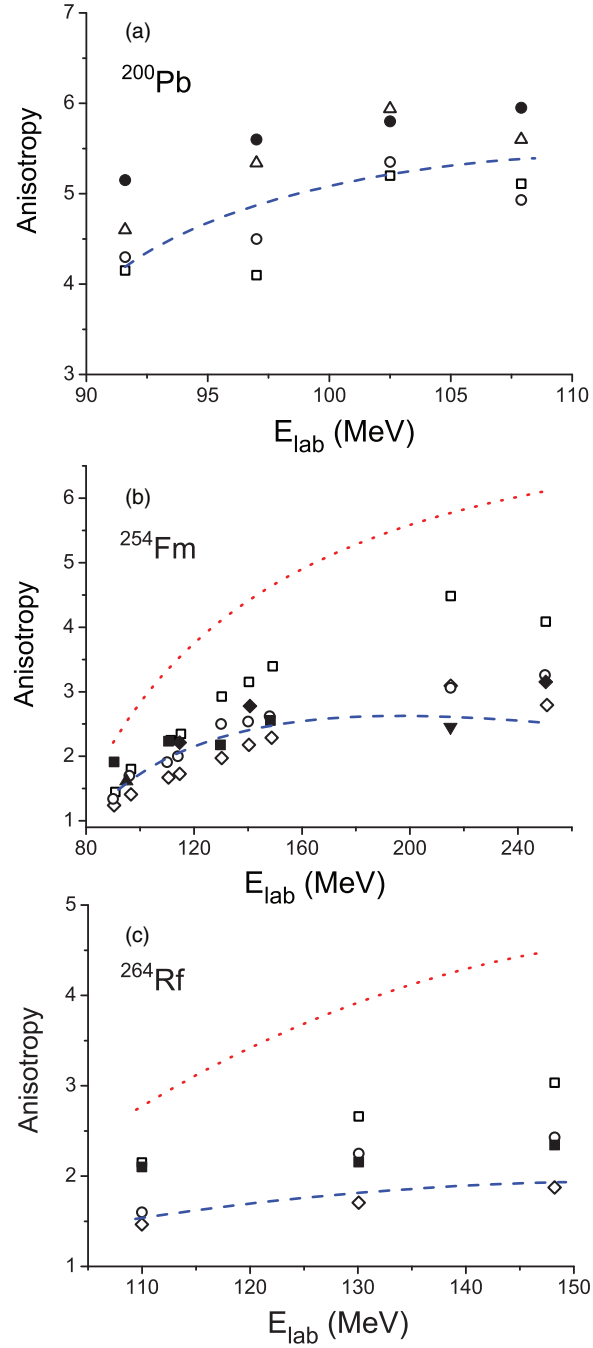

FIG. 12. (Color online) The anisotropy of fission fragment angular distribution for ^{200}Pb (a), ^{254}Fm (b), and ^{264}Rf (c). The experimental data are taken from Refs. [85] (filled squares), [86] (filled diamonds), [87] (filled triangle), [88] (filled inverted triangle), and [80] (filled circles). The 4D Langevin calculations were performed with $k_s = 0.25$ and $\gamma_K = 0.154$ $(\mathrm{MeV\,zs})^{-1/2}$ (open squares), $k_s = 0.35$ and $\gamma_K = 0.077$ $(\mathrm{MeV\,zs})^{-1/2}$ (open diamonds), deformation-dependent $k_s(q_1)$ and $\gamma_K = 0.2$ $(\mathrm{MeV\,zs})^{-1/2}$ (open triangles), and $k_s(q_1)$ and $\gamma_K = 0.077$ $(\mathrm{MeV\,zs})^{-1/2}$ (open circles). The dotted and dashed curves present the results predicted by the SCTS and SPTS models, respectively.

reasonably good agreement with the experimental data in the region of near-barrier and sub-barrier energies in the entrance channel of the reaction of heavy-ion collisions. Therefore,

development of a dynamical model for the evolution of the tilting mode with deformation-dependent and spin-dependent coefficient γ_K is desirable in the future. We also note that the theory of the transition state at the saddle point is inapplicable to some very heavy nuclei such as ^{254}Fm and ^{264}Rf that have fission barrier height comparable with the temperature of the compound nucleus.

IV. SUMMARY AND CONCLUSIONS

The 4D dynamical model [15], which has been proposed and developed on the basis of the 3D model [2,20,21] by incorporating the tilting degree of freedom (K coordinate) into Langevin dynamics, was systematically applied to the analysis of a wide set of observables from fusion-fission reactions induced by heavy ions. This 4D Langevin dynamical model makes it possible to calculate angular distribution of fission fragments together with the fission-fragment MED, the mean prescission particles multiplicity, the fission rate, and the fission time characteristics.

The proposed 4D dynamical model reproduces reasonably well the experimental parameters of the fission-fragment MED and the mean multiplicities of prescission neutrons over a wide range of the fissility parameter Z^2/A. In particular, the calculated variances of the mass distribution of fission fragments deviate from their experimental values by not more than 25% using the chaos-weighted wall formula with a deformation-dependent scaling factor from the wall formula $k_s(q_1)$ [51] for all considered nuclei in the present study. The use of the deformation-dependent factor $k_s(q_1)$ in dynamical calculations also leads to fairly good reproduction of the prescission neutron multiplicity for nuclei with $Z^2/A < 37$. For the heavier nuclei the larger values of k_s are needed for reproduction of the experimental $\langle n_{\rm pre}\rangle$ values. However, the inclusion of the K coordinate in the dynamical consideration and the consistent accounting of the influence of the K coordinate on the dynamical evolution of the shape degrees of freedom lead to the increase of $\langle n_{\rm pre}\rangle$ and σ_M^2 for heavy nuclei in the 4D Langevin calculations [15] with respect to the 3D ones. As a result, in the 4D calculations simultaneous reproduction of $\langle n_{\rm pre}\rangle$ and σ_M^2 is possible with almost similar k_s values, whereas in the 3D calculations for the heaviest nuclei $k_s \simeq 0.1$ was needed for the reproduction of σ_M^2 and $k_s > 1$ for the reproduction of $\langle n_{\rm pre}\rangle$. The present 4D calculations with deformation-dependent $k_s(q_1)$ could also reproduce the correlation dependencies $\langle n_{\rm pre}(M)\rangle$ and $\langle n_{\rm pre}(E_K)\rangle$ with the same quality as in 3D calculations [21].

The present 4D calculations demonstrate that the dissipation coefficient with respect to the K coordinate, $\gamma_K = 0.077$ $(\text{MeV zs})^{-1/2}$, found in Ref. [15] is reliable and allows reproduction of the parameters of angular distribution for heavy fissioning nuclei. The larger value $\gamma_K \simeq 0.2$ $(\text{MeV zs})^{-1/2}$ is needed for the lighter nucleus ^{200}Pb. In the present analysis we have found that the constant dissipation coefficient γ_K sometimes could not reproduce the anisotropy of the fission-fragment angular distribution; therefore, it is desirable to investigate the influence of a coordinate-dependent and spin-dependent coefficient γ_K on the calculated observables.

ACKNOWLEDGMENTS

We would like to thank Dr. C. Schmitt for useful collaboration, discussion, and correspondence. We are also grateful to Dr. D. O. Eremenko and Dr. A. V. Karpov for their continued interest in this study and many enlightening discussions and useful comments. Dr. S. V. Danilova is gratefully acknowledged for careful reading of the manuscript and suggestions that greatly improved the first version of the manuscript. This study was partially supported by the Russian Foundation for Basic Research, Research Project No. 13-02-00168 (Russia).

[1] Y. Abe, S. Ayik, P.-G. Reinhard, and E. Suraud, Phys. Rep. **275**, 49 (1996).
[2] G. D. Adeev, A. V. Karpov, P. N. Nadtochy, and D. V. Vanin, Phys. Part. Nucl. **36**, 378 (2005) [Fiz. Elem. Chastits At. Yadra **36**, 732 (2005)].
[3] J. Randrup and P. Möller, Phys. Rev. Lett. **106**, 132503 (2011).
[4] J. Randrup and P. Möller, Phys. Rev. C **88**, 064606 (2013).
[5] Y. Aritomo and S. Chiba, Phys. Rev. C **88**, 044614 (2013).
[6] G. D. Adeev and P. N. Nadtochy, Phys. At. Nucl. **66**, 618 (2003).
[7] H. Eslamizadeh, Eur. Phys. J. A **47**, 134 (2011).
[8] K. Mazurek, C. Schmitt, J. P. Wieleczko, P. N. Nadtochy, and G. Ademard, Phys. Rev. C **84**, 014610 (2011).
[9] H. Eslamizadeh, J. Phys. G: Nucl. Part. Phys. **39**, 085110 (2012).
[10] H. Eslamizadeh and H. Raanaei, Ann. Nucl. Energy **51**, 252 (2013).
[11] H. Eslamizadeh, J. Phys. G: Nucl. Phys. **40**, 095102 (2013).
[12] K. Mazurek, C. Schmitt, P. N. Nadtochy, M. Kmiecik, A. Maj, P. Wasiak, and J. P. Wieleczko, Phys. Rev. C **88**, 054614 (2013).
[13] J. P. Lestone, Phys. Rev. C **59**, 1540 (1999).
[14] J. P. Lestone and S. G. McCalla, Phys. Rev. C **79**, 044611 (2009).
[15] P. N. Nadtochy, E. G. Ryabov, A. E. Gegechkori, Y. A. Anischenko, and G. D. Adeev, Phys. Rev. C **85**, 064619 (2012).
[16] V. A. Drozdov, D. O. Eremenko, O. V. Fotina, S. Y. Platonov, and O. A. Yuminov, AIP Conf. Proc. **704**, 130 (2004)
[17] D. O. Eremenko, V. A. Drozdov, M. H. Eslamizadex, O. V. Fotina, S. Y. Platonov, and O. A. Yuminov, Phys. At. Nucl. **69**, 1423 (2006).
[18] A. V. Karpov, R. M. Hiryanov, A. V. Sagdeev, and G. D. Adeev, J. Phys. G: Nucl. Part. Phys. **34**, 255 (2007).
[19] R. M. Hiryanov, A. V. Karpov, and G. D. Adeev, Phys. At. Nucl. **71**, 1361 (2008).
[20] A. V. Karpov, P. N. Nadtochy, D. V. Vanin, and G. D. Adeev, Phys. Rev. C **63**, 054610 (2001).
[21] P. N. Nadtochy, G. D. Adeev, and A. V. Karpov, Phys. Rev. C **65**, 064615 (2002).
[22] A. E. Gegechkori and G. D. Adeev, Phys. At. Nucl. **74**, 1 (2011).
[23] Y. A. Anischenko, A. E. Gegechkori, and G. D. Adeev, Acta Phys. Pol. B **42**, 493 (2011).

[24] H. A. Kramers, Physica **7**, 284 (1940).
[25] H. J. Krappe, in *Proceedings of the XIII Meeting on Physics of Nuclear Fission in Memory of Prof. G. N. Smirenkin, Obninsk, 1995*, edited by B. D. Kuzminov (SSCRF-IPPE, Obninsk, 1995), pp. 134–144.
[26] P. Fröbrich and I. I. Gontchar, Phys. Rep. **292**, 131 (1998).
[27] M. Brack, J. Damgaard, A. S. Jensen, H. C. Pauli, V. M. Strutinsky, and C. Y. Wong, Rev. Mod. Phys. **44**, 320 (1972).
[28] A. Ignatyuk, M. G. Itkis, V. Okolovich, and G. Smirenkin, Sov. J. Nucl. **21**, 612 (1975).
[29] P. N. Nadtochy and G. D. Adeev, Phys. Rev. C **72**, 054608 (2005).
[30] H. J. Krappe, J. R. Nix, and A. J. Sierk, Phys. Rev. C **20**, 992 (1979).
[31] A. J. Sierk, Phys. Rev. C **33**, 2039 (1986).
[32] K. T. R. Davies, A. J. Sierk, and J. R. Nix, Phys. Rev. C **13**, 2385 (1976).
[33] J. Blocki, Y. Boneh, J. R. Nix, J. Randrup, M. Robel, A. J. Sierk, and W. J. Swiatecki, Ann. Phys. (NY) **113**, 330 (1978).
[34] J. Randrup and W. J. Swiatecki, Ann. Phys. (NY) **125**, 193 (1980).
[35] J. R. Nix and A. J. Sierk, in *Proceedings of the International School-Seminar on Heavy Ion Physics, Dubna, USSR, 1986*, edited by M. I. Zarubina and E. V. Ivashkevich (JINR, Dubna, 1987), pp. 453–464.
[36] J. R. Nix and A. J. Sierk, in *Proceedings of the 6th Adriatic Conference on Nuclear Physics: Frontiers of Heavy Ion Physics, Dubrovnik, Yugoslavia, 1987*, edited by N. Cindro, R. Caplar, and W. Greiner (World Scientific, Singapore, 1990), pp. 333–340.
[37] J. Randrup and W. J. Swiatecki, Nucl. Phys. A **429**, 105 (1984).
[38] T. Wada, Y. Abe, and N. Carjan, Phys. Rev. Lett. **70**, 3538 (1993).
[39] C. Schmitt, J. Bartel, K. Pomorski, and A. Surowiec, Acta Phys. Pol. B **34**, 1651 (2003).
[40] C. Schmitt, J. Bartel, A. Surowiec, and K. Pomorski, Acta Phys. Pol. B **34**, 2135 (2003).
[41] P. N. Nadtochy, A. V. Karpov, and G. D. Adeev, Phys. At. Nucl. **65**, 799 (2002).
[42] P. N. Nadtochy, A. V. Karpov, D. V. Vanin, and G. D. Adeev, Phys. At. Nucl. **66**, 1203 (2003).
[43] E. G. Ryabov, A. V. Karpov, P. N. Nadtochy, and G. D. Adeev, Phys. Rev. C **78**, 044614 (2008).
[44] J. J. Griffin and M. Dworzecka, Nucl. Phys. A **455**, 61 (1986).
[45] S. Pal and T. Mukhopadhyay, Phys. Rev. C **54**, 1333 (1996).
[46] T. Mukhopadhyay and S. Pal, Phys. Rev. C **56**, 296 (1997).
[47] S. Pal and T. Mukhopadhyay, Phys. Rev. C **57**, 210 (1998).
[48] J. Blocki, F. Brut, T. Srokowski, and W. J. Swiatecki, Nucl. Phys. A **545**, 511 (1992).
[49] J. Blocki, J.-J. Shi, and W. Swiatecki, Nucl. Phys. A **554**, 387 (1993).
[50] W. J. Swiatecki, Nucl. Phys. A **488**, 375c (1988).
[51] G. Chaudhuri and S. Pal, Phys. Rev. C **63**, 064603 (2001).
[52] K. T. R. Davies and J. R. Nix, Phys. Rev. C **14**, 1977 (1976).
[53] R. W. Hasse and W. D. Myers, *Geometrical Relationships of Macroscopic Nuclear Physics* (Springer-Verlag, Heidelberg, 1988), p. 116.
[54] T. Døssing and J. Randrup, Nucl. Phys. A **433**, 215 (1985).
[55] J. Randrup, Nucl. Phys. A **383**, 468 (1982).
[56] S. G. McCalla and J. P. Lestone, Phys. Rev. Lett. **101**, 032702 (2008).
[57] J. P. Lestone, A. A. Sonzogni, M. P. Kelly, and R. Vandenbosch, J. Phys. G: Nucl. Part. Phys. **23**, 1349 (1997).
[58] N. D. Mavlitov, P. Fröbrich, and I. I. Gontchar, Z. Phys. A **342**, 195 (1992).
[59] J. Marten and P. Fröbrich, Nucl. Phys. A **545**, 854 (1992).
[60] K. T. R. Davies, R. A. Managan, J. R. Nix, and A. J. Sierk, Phys. Rev. C **16**, 1890 (1977).
[61] R. Vandenbosch and J. R. Huizenga, *Nuclear Fission* (Academic, New York, 1973), p. 424.
[62] A. Bohr and B. R. Mottelson, *Nuclear Structure*, Vol. 2 (World Scientific, Singapore, 1998), p. 748.
[63] H. H. Rossner, J. R. Huizenga, and W. U. Schröder, Phys. Rev. Lett. **53**, 38 (1984).
[64] I. Halpern and V. M. Strutinsky, in *Proceedings of the Second United Nations International Conference on the Peaceful Uses of Atomic Energy, Geneva, Switzerland, 1957*, Vol. 15 (United Nations, Geneva, 1958), pp. 408–418.
[65] D. O. Eremenko, A. A. Dermenev, V. A. Drozdov, S. Y. Platonov, O. V. Fotina, and O. A. Yuminov, Bull. Russ. Acad. Sci.: Phys. **73**, 180 (2009).
[66] J. Randrup and T. Døssing, Nucl. Phys. A **428**, 255 (1984).
[67] R. Charity, M. McMahan, G. Wozniak, R. McDonald, L. Moretto, D. Sarantites, L. Sobotka, G. Guarino, A. Pantaleo, L. Fiore, A. Gobbi, and K. Hildenbrand, Nucl. Phys. A **483**, 371 (1988).
[68] D. J. Hinde, D. Hilscher, H. Rossner, B. Gebauer, M. Lehmann, and M. Wilpert, Phys. Rev. C **45**, 1229 (1992).
[69] A. Y. Rusanov, M. G. Itkis, and V. N. Okolovich, Phys. At. Nucl. **60**, 683 (1997).
[70] M. G. Itkis, Y. T. Oganessian, G. G. Chubarian, V. S. Salamatin, A. Y. Rusanov, and V. N. Okolovich, in *Proceedings of the EPS XV Nuclear Physics Divisional Conference on Low Energy Nuclear Dynamics (LEND-95), St Petersburg, Russia, April, 1995*, edited by Y. T. Oganessian, R. Kalpakchieva, and W. von Oertzen (World Scientific, Singapore, 1995), pp. 177–180.
[71] M. G. Itkis, S. M. Lukyanov, V. N. Okolovich, Y. E. Penionzkevich, A. Y. Rusanov, V. S. Salamatin, G. N. Smirenkin, and G. G. Chubaryan, Phys. At. Nucl. **52**, 15 (1990).
[72] G. G. Chubaryan, M. G. Itkis, and S. M. Lukianov, Phys. At. Nucl. **56**, 286 (1993).
[73] R. L. Ferguson, F. Plasil, H. Freiesleben, C. E. Bemis, and H. W. Schmitt, Phys. Rev. C **8**, 1104 (1973).
[74] P. N. Nadtochy, A. Kelić, and K.-H. Schmidt, Phys. Rev. C **75**, 064614 (2007).
[75] J. Sadhukhan and S. Pal, Phys. Rev. C **78**, 011603(R) (2008).
[76] M. Morjean *et al.*, Phys. Rev. Lett. **101**, 072701 (2008).
[77] D. Hilscher and H. Rossner, Ann. Phys. (Paris) **17**, 471 (1992).
[78] P. Nadtochy, A. Brondi, A. Di Nitto, G. La Rana, R. Moro, E. Vardaci, A. Ordine, A. Boiano, M. Cinausero, G. Prete, V. Rizzi, N. Gelli, and F. Lucarelli, EPJ Web Conf. **2**, 08003 (2010).
[79] J. O. Newton, D. J. Hinde, R. J. Charity, J. R. Leigh, J. J. M. Bokhorst, A. Chatterjee, G. S. Foote, and S. Ogaza, Nucl. Phys. A **483**, 126 (1988).
[80] J. S. Forster, I. V. Mitchell, J. U. Andersen, A. S. Jensen, E. Laegsgaard, W. M. Gibson, and K. Reichelt, Nucl. Phys. A **464**, 497 (1987).
[81] P. N. Nadtochy, E. G. Ryabov, A. E. Gegechkori, Y. A. Anischenko, and G. D. Adeev, EPJ. Web. Conf. **62**, 07001 (2013).

[82] F. Plasil, D. S. Burnett, H. C. Britt, and S. G. Thompson, Phys. Rev. **142**, 696 (1966).
[83] J. R. Nix and W. J. Swiatecki, Nucl. Phys. **71**, 1 (1965).
[84] J. R. Nix, Nucl. Phys. A **130**, 241 (1969).
[85] B. B. Back, R. R. Betts, J. E. Gindler, B. D. Wilkins, S. Saini, M. B. Tsang, C. K. Gelbke, W. G. Lynch, M. A. McMahan, and P. A. Baisden, Phys. Rev. C **32**, 195 (1985).
[86] A. Gavron *et al*., Phys. Rev. Lett. **52**, 589 (1984).
[87] J. Tōke, R. Bock, G.-X. Dai, A. Gobbi, S. Gralla, K. D. Hildenbrand, J. Kuzminski, W. F. J. Müller, A. Olmi, W. Reisdorf, S. Børnholm, and B. B. Back, Phys. Lett. B **142**, 258 (1984).
[88] L. C. Vaz, D. Logan, E. Duek, J. M. Alexander, M. F. Rivet, M. S. Zisman, M. Kaplan, and J. W. Ball, Z. Phys. A **315**, 169 (1984).
[89] M. G. Itkis, Y. A. Muzychka, Y. T. Oganessian, V. N. Okolovich, V. V. Pashkevich, A. Y. Rusanov, V. S. Salamatin, G. N. Smirenkin, and G. G. Chubarian, Phys. At. Nucl. **58**, 2026 (1995).
[90] M. G. Itkis and A. Y. Rusanov, Phys. Part. Nucl. **29**, 160 (1998).
[91] O. I. Serdyuk, G. D. Adeev, I. I. Gonchar, V. V. Pashkevich, and N. I. Pischasov, Sov. J. Nucl. Phys. **46**, 399 (1987).
[92] G. D. Adeev, I. I. Gonchar, V. V. Pashkevich, N. I. Pischasov, and O. I. Serdyuk, Sov. J. Part. Nucl. **19**, 529 (1988) [Fiz. Elem. Chastits At. Yadra **19**, 1229 (1988)].
[93] G. Adeev and V. Pashkevich, Nucl. Phys. A **502**, 405c (1989).
[94] Y. A. Anischenko and G. D. Adeev, Phys. At. Nucl. **75**, 933 (2012).
[95] M. V. Borunov, P. N. Nadtochy, and G. D. Adeev, Nucl. Phys. A **799**, 56 (2008).
[96] M. V. Borunov, P. N. Nadtochy, and G. D. Adeev, Phys. At. Nucl. **70**, 1846 (2007).
[97] H. Rossner, J. R. Huizenga, and W. U. Schröder, Phys. Rev. C **33**, 560 (1986).
[98] B. John and S. K. Kataria, Phys. Rev. C **57**, 1337 (1998).
[99] B. B. Back, H. G. Clerc, R. R. Betts, B. G. Glagola, and B. D. Wilkins, Phys. Rev. Lett. **46**, 1068 (1981).
[100] P. D. Bond, Phys. Rev. C **32**, 471 (1985).
[101] P. D. Bond, Phys. Rev. C **32**, 483 (1985).
[102] H. Rossner, D. Hilscher, E. Holub, G. Ingold, U. Jahnke, H. Orf, J. R. Huizenga, J. R. Birkelund, W. U. Schröder, and W. W. Wilcke, Phys. Rev. C **27**, 2666 (1983).
[103] S. Cohen, F. Plasil, and W. J. Swiatecki, Ann. Phys. (NY) **82**, 557 (1974).
[104] R. Freifelder, M. Prakash, and J. M. Alexander, Phys. Rep. **133**, 315 (1986).
[105] V. A. Drozdov, D. O. Eremenko, S. Y. Platonov, O. V. Fotina, and O. A. Yuminov, Phys. At. Nucl. **64**, 179 (2001).
[106] V. S. Ramamurthy and S. S. Kapoor, Phys. Rev. Lett. **54**, 178 (1985).
[107] M. A. Butler, S. S. Datta, R. T. de Souza, J. R. Huizenga, W. U. Schröder, J. Töke, and J. L. Wile, Phys. Rev. C **34**, 2016 (1986).
[108] J. O. Newton, Fiz. Elem. Chastits At. Yadra **21**, 821 (1990).
[109] R. G. Thomas, R. K. Choudhury, A. K. Mohanty, A. Saxena, and S. S. Kapoor, Phys. Rev. C **67**, 041601 (2003).
[110] H. Q. Zhang, Z. H. Liu, J. C. Xu, M. Ruam, C. J. Lin, and X. Qian, J. Nucl. Radiochem. Sci. **3**, 99 (2002).
[111] V. A. Drozdov, D. O. Eremenko, O. V. Fotina, S. Y. Platonov, O. A. Yuminov, D. Mandaglio, M. Manganaro, and G. Fazio, Int. J. Mod. Phys. E **19**, 1125 (2010).
[112] Z. H. Liu, H. Q. Zhang, J. Xu, Y. Qiao, X. Qian, and C. Lin, Phys. Lett. B **353**, 173 (1995).